Amino-polyvinyl Alcohol Coated Superparamagnetic Iron Oxide Nanoparticles are Suitable for Monitoring of Human Mesenchymal Stromal Cells In Vivo

Frank Schulze, Anke Dienelt, Sven Geissler, Paul Zaslansky, Janosch Schoon, Katja Henzler, Peter Guttmann, Azza Gramoun, Lindsey Crowe, Lionel Maurizi, et al.

DOI: 10.1002/ ((please add manuscript number))
Article type: Full Paper

Title

Amino-polyvinyl alcohol coated superparamagnetic iron oxide nanoparticles are suitable for monitoring of human mesenchymal stromal cells *in vivo*

Authors

Frank Schulze, Anke Dienelt, Sven Geissler, Paul Zaslansky, Janosch Schoon, Katja Henzler, Peter Guttmann, Azza Gramoun, Lindsey A. Crowe, Lionel Maurizi, Jean-Paul Vallée, Heinrich Hofmann, Georg N. Duda, Andrea Ode*

Frank Schulze, Dr. Anke Dienelt, Dr. Sven Geissler, Dr. Paul Zaslansky, Janosch Schoon, Prof. Georg N. Duda, Dr. Andrea Ode
Julius Wolff Institute, Charité – Universitätsmedizin Berlin, 13353 Berlin, Germany
E-mail: georg.duda@charite.de

Dr. Katja Henzler, Dr. Peter Guttmann
Institute for Soft Matter and Functional Materials, Helmholtz-Zentrum für Materialien und Energie GmbH, 14109 Berlin, Germany

Dr. Azza Gramoun, Dr. Lindsey A. Crowe, Prof. Jean-Paul Vallée
Department of Radiology, Geneva University Hospitals and University of Geneva, 1205 Geneva, Switzerland

Dr. Lionel Maurizi, Prof. Heinrich Hofmann
Laboratory of Powder Technology, Ecole Polytechnique Fédérale de Lausanne (EPFL), 1015 Lausanne, Switzerland

Keywords: mesenchymal stromal cells, superparamagnetic iron oxide nanoparticles, polyvinylalcohol, magnetic resonance imaging, cell based therapies

Abstract

Mesenchymal stromal cells (MSCs) are promising candidates in regenerative cell-therapies. However, optimizing their number and route of delivery remains a critical issue, which can be addressed by monitoring the MSCs' bio-distribution *in vivo* using super-paramagnetic iron-oxide nanoparticles (SPIONs).

In this study, amino-polyvinyl alcohol coated (A-PVA) SPIONs were introduced for cell-labelling and visualization by magnetic resonance imaging (MRI) of human MSCs.

Size and surface charge of A-PVA-SPIONs differed depending on their solvent. Under MSC-labeling conditions, A-PVA-SPIONs had a hydrodynamic diameter of 42 ± 2 nm and a negative Zeta potential of 25 ± 5 mV, which enabled efficient internalization by MSCs without the need to use transfection agents. Transmission X-ray microscopy localized A-PVA-SPIONs in intracellular vesicles and as cytosolic single particles. After identifying non-interfering cell-assays and determining the delivered and cellular dose, in addition to the administered dose, A-PVA-SPIONs were found to be non-toxic to MSCs and non-destructive towards their multi-lineage differentiation potential. Surprisingly, MSC migration was increased. In MRI, A-PVA-SPION-labelled MSCs were successfully visualized *in vitro* and *in vivo*.

In conclusion, A-PVA-SPIONs had no unfavorable influences on MSCs, although it became evident how sensitive their functional behavior is towards SPION-labeling. And A-PVA-SPIONs allowed MSC-monitoring *in vivo*.

1. Introduction

Mesenchymal stromal cells (MSCs) have gained much interest as a promising source for cell-based therapies. Their potential to regenerate damaged tissue has been attributed to their ability of self-renewal, differentiation into a variety of specialized cell types (e.g. in bone MSCs are able to differentiate into bone-forming osteoblasts) and migration towards gradients of growth factors secreted by damaged tissue.[1] Experimental cell-therapy approaches in animals using MSCs led to promising results for a number of neurological, myocardial and musculoskeletal disorders (e.g. femoral head necrosis, osteogenesis imperfecta, and osteoarthritis).[2-7] Even though numerous clinical trials have been initiated and some revealed a degree of success, a broad clinical application of such therapies is still not available.[8, 9] Critical parameters for successfully transferring results from animal experiments to clinical application include the number of transplanted cell and their cultivation and delivery process. Visualizing and monitoring the temporal and spatial distribution of transplanted cells can provide valuable insight into understanding how to optimize cell delivery and/or dosing. Unfortunately, methods for non-invasive tracking of transplanted cells *in vivo* are still limited.

Visualization of cells *in vivo* can be achieved by using different molecular imaging modalities such as magnetic resonance imaging (MRI), radionuclide imaging (positron emission tomography (PET), single-photon emission computed tomography (SPECT)) and optical imaging.[10, 11] Although none of these imaging techniques is optimal, MRI is still the preferred imaging modality for visualization of exogenously delivered cells, because of its non-destructive and non-invasiveness, deep penetration and high spatial resolution.[12]

The most commonly used imaging agents for MRI application are superparamagnetic iron-oxide nanoparticles (SPIONs), which were introduced several decades ago and have become a part of daily clinical routine use such as in imaging liver metastasis. SPIONs are nanoscaled

(5 - 15nm) crystals that consist of the biodegradable iron oxides magnetite (Fe_3O_4) or maghemite (γ-Fe_2O_3) or a mixture of both phases and exhibit magnetism only under the influence of an external magnetic field (superparamagnetism).[13] In MRI, SPIONs exhibit a negative enhancement on T2- and T2* weighted sequences, thus generating a signal change that is several magnitudes stronger compared to other contrast agents (e.g. gadolinium).[14] To improve colloidal stability, solubility, and biocompatibility, SPIONs are coated with polymers such as dextran.[15]

Most previous studies on cellular tracking of MSCs used commercially available dextran- or carboxydextran-coated SPIONs (Endorem/Feridex or Resovist, respectively).[16-22] However, manufacturing of both products was discontinued in 2008 and 2009, which prevents their future applications. But more importantly, these nanoparticles were originally developed to be taken up by phagocytic cells from the reticuloendothelial system (e.g. monocytes, macrophages and osteoclasts) but not by non-phagocytic cells such as MSCs. To overcome this limitation, transfection agents (TA) were used.[23] However, some TAs are reported to be toxic under certain circumstances and their influence on MSCs biology is an issue of debate.[19, 24-26] In addition, the colloidal stability of dextran- or carboxydextran-coated SPIONs is impaired in cell culture media, making *in vitro* labeling difficult.[27] ~~Furthermore, the dextran-coating itself raises problems as it is susceptible to lysosomal degradation, resulting in exposure of cellular compartments and the cytosol to uncoated iron oxide nanoparticles and ions causing cytotoxic effects.[27, 28]~~ Therefore, it is necessary to develop SPIONs with non-toxic coatings that meet the physiochemical need for efficient cellular uptake by MSCs *in vitro*.

In recent years, several studies focused on the development of novel SPION-coatings for MSC-labeling.[28-33] Unfortunately, most of the previous studies suffer from missing information on either one or more of the following aspects: (1) characterization of the physiochemical properties of SPIONs, (2) exclusion of SPION-interference with the applied

methods (especially fluori- and colorimetric toxicity assays), (3) proof of SPION-internalization, (4) information on the correct dosimetry, which includes not only the administered, but also the delivered and effective cellular dose, (5) analysis of possible secondary effects introduced by SPIONs on MSC beyond their key characteristics and (6) the proof of principle for MRI visualization of SPION-labeled MSCs *in vitro* and *in vivo*. It is thus difficult to accurately interpret the results and compare them between different studies.

In this study, we describe a novel approach to address the above-mentioned challenges. Our aim was to label MSCs with amino-polyvinyl alcohol coated SPIONs (A-PVA-SPIONs) and to find a balance between cellular uptake without TAs for MRI visualization and low toxicity/impact on MSC cellular functionality. In particular, we aim (1) to develop an efficient A-PVA-SPION-labeling procedure for MSCs based on particle internalization, (2) to analyze the influence of A-PVA-SPIONs on MSC viability, proliferation, adipogenic, osteogenic and chondrogenic differentiation as well as migration and (3) to provide proof of principle for visualization of A-PVA-SPION-labeled MSCs in MRI *in vitro* by using MRI-phantoms and *in vivo* by using animal models. We hypothesize that A-PVA-SPIONs are suitable to label MSCs without provoking cytotoxicity allowing their visualization and monitoring in MRI.

2. Results

2.1. Development of an efficient A-PVA-SPION-labeling procedure for MSCs

Developing an efficient A-PVA-SPION labeling procedure is crucial for subsequent visualization of MSCs in MRI and requires information about the nanoparticles physiochemical properties. For example, the extent to what nanoparticles are internalized by cells is determined by characteristics like size and surface charge, i.e. hydrodynamic diameter and Zeta potential.[15] Furthermore, the size of the nanoparticle is needed for dosimetry calculations and for correct identification when confirming internalization by nanoscale-resolution imaging methods. The physiochemical properties of polymer coated SPIONs can change in response to pH (i.e. osmotic swelling) and protein concentration (i.e. formation of protein corona).[49] It is thus important to thoroughly characterize the A-PVA-SPIONs under conditions that are identical to the read-out experiments.[50] Therefore, we characterized size and surface charge of A-PVA-SPIONs not only in their solvent (HNO_3 10mM, pH 2) but also in cell culture media (physiological pH 7.4) with and without fetal calf serum (FCS) supplementation. The iron oxide crystal mean diameter was 7.2 ± 2.5 nm (~~Figure S1~~Figure 1). The SPIONs hydrodynamic diameter measures 14 ± 2 nm for the uncoated and 25 ± 3 nm for the A-PVA-coated SPION in its solvent HNO_3 (10mM, pH2). The Zeta potential of the uncoated SPIONs is at 26 ± 2 mV and slightly decreases to 20 ± 2 mV when the A-PVA-coating is added. When transferred into FCS-free DMEM, the A-PVA-SPIONs hydrodynamic diameter increases to 42 ± 2 nm, in the presence of FCS to 45 ± 2 nm. The addition of FCS to the cell culture media results in a negative shift in the Zeta potential of A-PVA-SPIONs from 21 ± 5 mV to -25 ± 5 mV (summarized in ~~Table S1~~Table 1). Both, the increased hydrodynamic diameter and the negative zeta potential confirm the adsorption of proteins.[51] In conclusion, we now expect intracellular A-PVA-SPIONs with a diameter of 42 ± 2 nm to 45 ± 2 nm in the following experiments proving their internalization. In addition, the

determined size of 45 ± 2 nm will be the basis for calculating the A-PVA-SPIONs colloidal behavior that is needed for establishing a dosimetry (details see **Table S1**).

We then investigated whether A-PVA-SPIONs are internalized by MSCs without any external support such as transfection agents or magnetic fields. To confirm cellular internalization, we used methods beyond Prussian Blue staining that allow resolution in the nanoscale: transmission electron microscopy (TEM) and transmission X-ray microscopy (TXM). For this purpose, MSCs were incubated for four hours with A-PVA-SPIONs (100µg$_{Fe}$/ml) under serum-deprived conditions, which is known to be beneficial for efficient internalization.[53] The qualitative assessment of A-PVA-SPION internalization was facilitated by TEM and TXM. TEM revealed that A-PVA-SPIONs are internalized by MSCs and stored in intracellular vesicles (mean vesicle diameter: 357 ± 68.4 nm) (**Figure 2**). TXM supported these findings (mean vesicle diameter: 387 ±48.4 nm) and provided additional information that A-PVA-SPIONs are also found in smaller high contrast spheres (mean sphere diameter: 52 ± 9.2 nm), clusters of irregular shape, and a micron-sized cluster (length: 2000 nm; width: 291 nm) in the cytoplasm (**Figure 3 and see also Video S1**).

After having proven that A-PVA-SPIONs are internalized by MSCs, we sought experimental conditions to optimize their cellular dose and define the corresponding dosimetry. Reporting a comprehensive dosimetry that consists of the administered, delivered and cellular dose is crucial for the establishment of a correct dose-response relationship.[53] The administered dose itself only describes the amount of nanoparticles that was employed at the beginning of the experiment. A more relevant metric is described by the delivered dose that also takes the particles colloidal behavior and the exposure time into account and gives thus information about the amount of particles that reaches the cell monolayer.[34] Finally the cellular dose can be determined experimentally and describes the amount of A-PVA-SPIONs internalized by the cells. For this, MSCs were incubated with varying concentrations of A-PVA-SPIONs (administered dose) and the corresponding cell-bound iron (cellular dose) was determined.

After four hours, the value for cell-bound iron reaches 5.9 ± 2.5 pg_{Fe}/cell at the lowest administered dose (50µg Fe/ml), which does not further increase significantly at higher administered doses. The TA Protamine had no beneficial effect (ANOVA, p=0.126) on this pattern (**Figure 4A**). However, when incubation time was extended to 24 hours, an increase of cell-bound iron was observed (ANOVA, p=0.014). After 24 hours, the cell-bound iron increases to 8.2 ± 3.6 pg_{Fe}/cell at the lowest administered dose (50μg_{Fe}/ml), which is again not affected by increasing the administered dose (**Figure 4B**). For accurate interpretation of the results and comparability with other studies, a summary of the particle dosimetry results is given in **Table 2**. In summary, we found that an optimized cellular dose in MSCs is reached at A-PVA-SPION-labeling for 4h under serum-deprived conditions followed by 20h under standard MSC culture conditions without the need of additional Protamine as TA.

2.2. Non-toxic A-PVA-SPIONs stimulate MSCs migration

When using A-PVA-SPIONs for MSC-labeling in cell-based therapy approaches, compromising effects on MSC survival and function have to be avoided. We thus investigated viability, multilineage differentiation and migration of MSCs after A-PVA-SPION-labeling with four different administered doses ranging from 0 to 100μg_{Fe}/ml.

Viability and proliferation of A-PVA-SPION-labeled MSCs was assessed after four and eight days and found to be unaffected compared to unlabeled MSCs (**Figure 5**). Notably, the amount of cell bound iron is below the critical value that leads to interference with these assays (**Figure S2 and Information S3**). Differentiation of A-PVA-SPION-labeled MSCs towards the adipogenic, osteogenic, and chondrogenic phenotype was achieved without differences to their respective controls (**Figure 6**). Migration was analyzed in a modified wound scratch assay. A-PVA-SPION-labeled MSCs exhibit an increase in migration rate compared to unlabeled controls (**Figure 7 and Video S2 and S3**). Quantitative analysis revealed that this effect reaches statistical significance at the highest analyzed A-PVA-SPION

concentration (50µg$_{Fe}$/ml *vs.* control: p=0.069; 100µg$_{Fe}$/ml *vs.* control: p=0.001; Figure 7). Our results show that A-PVA-SPION-labeling does not affect differentiation, a key function of MSCs as defined by The International Society for Cellular Therapy (ISCT), but rather stimulates their migratory behavior.[35]

2.3. A-PVA-SPION-labeled MSCs can be visualized in MRI *in vitro* and *in vivo*

We found that labeling of MSCs with A-PVA-SPIONs had no negative effects on their viability or regenerative and therefore we investigated whether the amount of cell-bound iron was sufficient for visualization of A-PVA-SPION labeled MSCs using MRI *in vitro* and *in vivo*. To this end, cell phantoms with different numbers of A-PVA-SPION-labeled MSCs were prepared and scanned by MRI using T2 STIR and T1 VIBE sequences. A small effect could be seen using both sequences where a signal loss due to the A-PVA-SPION labeled MSCs was detected only at the highest cell concentration on the transverse plane of the MR images (**Figure 8A**). Acquisition of the orthogonal plane showed that the cells were concentrated at the bottom of the wells (data not shown). However, due to the small depth of the gel, which was lower than the minimum slice thickness available, the meniscal 'partial volume' effect precluded any quantification. Cell distribution was not homogenous enough to determine a precise effect of cell number on T1 and T2 star relaxation times. Nonetheless, the phantom results showed a trend in effect on T2 and indicated that MSC labeling was efficient for MRI visualization with the sequences used.

In vivo, A-PVA-SPION induced signal loss was detectable on T1 weighted (VIBE) MR images as a black region superior and anterior to the lower section of the femur 24 hours after the injection of the A-PVA-SPION-labeled MSCs into the right naïve knee joint of Lewis rats (**Figure 8B I, III**). No signal could be seen at the region on VIBE MR images of the left knee joint where non-labeled MSCs were injected (**Figure 8C I and III**). These findings were confirmed using corresponding dUTE MR images where A-PVA-SPION-labeled MSCs result

234 in positive MR enhancement and can be seen as a white region at the same position which is
235 absent in controls (**Figure 8B II, IV and 8C II, IV**). Post mortem histology of the animal's
236 knee joints confirmed the presence of A-PVA-SPION labeled MSCs (**Figure S3**).
237
238

3. Discussion

Our aim in this study was to develop an efficient labeling procedure for human MSCs with A-PVA-SPIONs bypassing detrimental secondary effects on MSC viability and functions and verifying the feasibility of visualizing A-PVA-SPION-labeled MSCs in MRI.

3.1. Development of an efficient labeling procedure

A major advantage of PVA is the fact that it is biocompatible and safe to use in humans as it has been in medical use for several years, such as for cartilage replacements, wound packing and contact lenses.[54] A-PVA-SPIONs are already well characterized for their physiochemical and magnetic properties.[55] In contrast to dextran- or carboxydextran-SPIONs, they exhibit excellent colloidal stability and dispersion in different cell culture media *in vitro* even in the presence of fetal calf serum (FCS).[52] The amine-functionalization promotes A-PVA-SPION internalization by non-phagocytic cells without the need for compromising TAs , which also applies for primary human cells such as MSCs as proven in our study. [38, 56, 57]

Evidence of the internalization of A-PVA-SPIONs by MSCs and their subcellular location was provided by both TEM and TXM approaches. The advantages of the TXM approach over methods used in other studies are artifact-free sample preparation of the MSCs, visualization in the nanometer range and 3D spatial information, i.e. conclusive evidence of cellular internalization. The TEM approach showed A-PVA-SPIONs as high contrast particles that accumulate in intracellular vesicles. The TXM data confirmed this result, but also demonstrated that smaller high contrast spheres and irregular shaped clusters can be found. The size of these small high contrast spheres analyzed by TXM is similar to the size of A-PVA-SPIONs in DMEM + FCS determined by PCS (TXM: 52.9 ±9 nm vs. PCS: 45 ± 2nm). We thus assume that single A-PVA-SPIONs are either internalized individually or are a result of endosomal escapes. So far, we cannot distinguish whether the single A-PVA-SPIONs are either vesicle-bound or freely dispersed in the cytosol. Vesicle-bound single particles would

indicate that A-PVA-SPIONs enter via a typical endocytosis-exocytosis route by being internalized as individual nanoparticles and further sorted into bigger vesicles like lyso- or exosomes.[58] Freely dispersed A-PVA-SPIONs could directly interact with constituents of the cytosol, i.e. proteins, mRNA, and cellular organelles, which may be other avenues of A-PVA-SPION-induced functional changes. However, further research is needed to provide conclusive evidence for one of those assumptions. Quantitative assessment of the cellular dose revealed that a higher amount of cell-bound iron can be achieved by prolonging the incubation time, but not by increasing the administered dose above 50µg_{Fe}/ml. Similar results were already observed for the internalization of PVA-SPIONs by non-phagocytic cell lines.[38, 57] These results point towards an active uptake mechanism, which is energy dependent as recently suggested.[52] A more detailed discussion of the dosimetry can be found in **Information S4**.

3.2. Analysis of possible secondary effects

For MSC tracking approaches *in vivo*, it is important that those A-PVA-SPIONs are not only non-toxic, but also do not interfere with the cells' regenerative functions. Therefore, we first focused on proliferation and multi-lineage differentiation both are key functions of MSCs as defined by The International Society for Cellular Therapy (ISCT).[35]

In our study, we observed no signs of A-PVA-SPION-induced toxicity as proliferation and mitochondrial activity were unchanged similar to results observed for other cells.[52, 57] Next, the MSCs' ability to differentiate into the adipogenic, osteogenic and chondrogenic lineage was investigated and was found to be unchanged. These positive results are noteworthy since a number of studies reported impaired chondrogenesis after SPION-application.[18, 19, 25, 59] Only two of these publications report the corresponding cellular doses that were higher than the one determined in our study; 25.7 ± 0.96 pg_{Fe}/cell and 13 – 16 pg_{Fe}/cell.[19, 25] The impairment of chondrogenesis might thus be caused by a high intracellular iron load as

already hypothesized.[18, 25] It can be thus assumed that the cellular dose of 8.2 ± 3.6 pg/cell in our study is below a critical threshold that leads to impaired chondrogenesis.

A number of *in vivo* studies provide evidence that exogenously delivered MSCs migrate and target specific tissues via an active mechanism. For example, when injected into femurs MSCs were later detected in the contralateral bone or MSCs implanted into the tibial bone marrow cavity were detected in the callus of the ulnar fracture site after three weeks.[60, 61] Three days after injection into the tail-vein MSCs were detected at the fracture site.[62] Interestingly, in our study, migration of MSCs is increased after labeling with A-PVA-SPIONs. This effect could be advantageous in the context of cell-based therapies as exogenously delivered MSCs might migrate better *in vivo*. On the other hand, this effect could also be disadvantageous as it indicates cellular changes by A-PVA-SPIONs in MSCs that could influence so-far unknown parameters beyond migration. Future studies are needed to determine if the change in migration upon A-PVA-SPION-labeling has consequences for the outcome of MSC-based therapies.

4. Conclusion

SPION-labeling in combination with MRI is still the most promising approach for *in vivo* visualization of exogenously delivered cells and has gained high interest in cell-based therapies using MSCs. In the current study, we characterized the physiochemical properties of A-PVA-SPIONs, investigated their interference with viability assays and their internalization by human MSCs, report a correct dosimetry, found no impact on MSC viability and differentiation, but enhanced migration, and finally provided the proof of principle for MRI visualization of A-PVA-SPION-labeled MSCs *in vitro* and *in vivo*. The current study thus provides comprehensive information about the impact of A-PVA-SPIONs on MSCs and the feasibility of MRI visualization. In summary, the A-PVA/PVA copolymer has proven to be a suitable SPION-coating used for MSC labeling. What remains unknown is the particles' long-term fate with respect to MRI visualization of A-PVA-SPION labeled MSCs. For example, the accuracy of MRI data *in vivo* is compromised by the inability to distinguish signals (1) from viable and dead cells, (2) from internalized and excreted SPIONs and (3) from SPIONs and MSCs engulfed by macrophages. Another concern is the A-PVA-SPIONs metabolism within the body that is determined by its stability *in vivo*. Future work should therefore focus on research addressing 1) the A-PVA-SPIONs' retention time in the cell and elucidation of the involved endo- and exocytosis mechanisms and 2) whether the A-PVA-coating separates from the iron core resulting in renal excretion of A-PVA and integration of the SPION's iron in the body's iron metabolism. Taken together, these data help to develop A-PVA-SPION-based MRI-tracking of MSCs towards a reliable research tool where non-invasiveness, deep penetration, and high spatial resolution are needed. Thereby, it might be possible to gain further insight into the spatial and temporal distribution of transplanted MSCs in tissue repair and thus to optimize cell-based therapies.

334

5. Experimental Section

SPION synthesis and A-PVA surface modification: A-PVA-SPION. SPIONs were synthesized following a co-precipitation protocol.[36, 37] Briefly 0.064 moles of iron II from $FeCl_2$ and 0.128 moles of iron III from $FeCl_3$ were solved in 1.5 L deionized (DI) water and mixed with 120 mL of an NH_4OH solution (25%). After 10 min the suspension was sedimented under a magnetic field and washed with DI water until pH 7. SPIONs were redispersed in 400 mL and oxidized with 160 mL HNO_3 (2M) and 240 mL $Fe(NO_3)_3$ (0.35M) under reflux for 1.5h to achieve maghemite (γ-Fe_2O_3). The suspension was washed again with DI water and was dialyzed (with MWCO 12-14 kDa cellulose membrane dialysis tubing) against HNO_3 (10mM) for 3 days by changing the solution every 12h. The suspension was finally centrifuged at 30000 g for 15 min and the supernatant was kept. The final suspension of SPION had a concentration of 10 mg_{Fe}/mL and a pH of approximately 2. Surface modification of the SPION with PVA was done following a protocol described previously.[36, 38, 39] PVA-OH (10 wt%; Mowiol 3-85, Kuraray Europe GmbH) and A-PVA (2 wt %; M12, Erkol.) solutions were prepared by dissolving dry PVA in ultrapure DI water and the solutions were rapidly heated for 1 hour at 90°C, cooled down, filtered at 0.45 µm with a PTFE filter syringe and stored at 4°C. 10 volumes of naked SPION were mixed with 9 volumes of PVA-OH solution (100 mg PVA OH/mL) and 1 volume of A-PVA solution (20 mg A-PVA/mL). The final A-PVA-SPION suspension (5 mg_{Fe}/mL, pH 3) was stored at least 1 week at 4°C before further use.

A-PVA-SPION characterization: Crystallite's size was measured by counting of 400 crystallites sizes on Transmission Electron Microscopy (TEM CM12; FEI Co. Philips Electron Optics, Zürich, Switzerland) pictures. Hydrodynamic diameters and Zeta potential of A-PVA-SPIONs were measured on a Photon Correlation Spectroscopy apparatus (PCS

ZetaPals from Brookhaven: Laborchemie GES.M.B.H., Vienna, Austria). Uncoated SPIONs and A-PVA-SPION suspension were investigated by Fourier Transformation InfraRed spectroscopy (FTIR) showing the characteristic vibration bands for γ-Fe2O3 and A-PVA (Figure S1 and Information S2).

Human MSC isolation, cultivation and functional analysis: This study was approved by the local ethical committee; all donors gave informed written consent. Primary human MSCs were isolated from bone marrow of human donors (8 male, mean age: 59 ± 9.1 years; 7 female, mean age: 60 ± 16.6 years) undergoing hip surgery as described previously.[40] The "culture medium" was Dulbecco's modified Eagle's medium (DMEM; Low Glucose, Gibco, Grand Island, NY) with 10% fetal calf serum (FCS; Biochrom AG, Berlin, Germany), 5mM L-alanyl-L-glutamine (Gibco, Grand Island, NY), 100 U/mL penicillin plus 100 µg/mL streptomycin. Cells were counted by using CasyTT for standard cell culture (Schärfe Systems, Reutlingen, Germany) or a Neubauer chamber (C-Chip, Peqlab, Erlangen, Germany) when only small volumes of cells were available. All experiments described in this section where performed with cells from n=5 individual donors.

Proliferation rates were assessed by using a CyquantNF® Cell Proliferation assay kit (Life Technologies, Carlsbad, CA, United States). Cell viability was assessed using PrestoBlue® (Life Technologies, Carlsbad, CA, United States) as described earlier.[41] Briefly, 2000 MSCs/cm^2 were seeded into 48-well plates and measured after one (d1), four (d4) and eight (d8) days of culture. CyquantNF® values from d4 and d8 were normalized to d1. PrestoBlue® values were normalized to cell number determined by CyquantNF®. All measurements were performed in triplicates using a multimode microplate reader (m200 pro, Tecan).

Osteogenic differentiation of 2.4 x 10^4 MSCs per 24-well was induced by supplementing culture media with 200 µM ascorbic acid, 7 mM ß-glycerol phosphate, 0.01 µM

dexamethasone for 13 d. The calcified matrix was visualized by Alizarin Red S (AR) and quantified photometrical by dissolving AR in 10% cetylpyridinium chloride (readout wavelength at λ=562nm). Adipogenic differentiation was induced by supplementing culture media with 1 µM dexamethasone, 2 µM insulin, 200 µM indomethacin, 500 µM isobutyl-methyl-xanthin for 14 d. Fatty acids were detected by OilRed O staining and quantified photometrical by dissolving in 100% isopropanol (readout wavelength at λ=500nm). Each experiment was conducted in triplicate. Chondrogenesis was induced by stimulating a pellet culture (3 x 10^5 cells/pellet) with FCS-free culture media plus 10 ng/mL TGF-β1, 10–7 M dexamethasone, 50 µg/mL ascorbic acid, 40 µg/mL proline, 100 µg/mL pyruvate, 6.25 µg/mL ITS, 1.25 mg/mL BSA, 5.35 mg/mL linoleic acid) for 21 d and detected by Alcian Blue staining and quantification of proteoglycan as described elsewhere with the modification for pellet cultures and optimized read out wavelength (λ= 516nm).[42]

Migration was analyzed in culture inserts for self-insertion (IBIDI, Munich, Germany) in duplicate. 8x10^3 cells were allowed to attach for 5h in each cavity of the insert prior to insert removal and addition of culture media with 5µg/ml Mitomycin C (Sigma-Aldrich, St. Louis, USA). Migration into the defined cell free gap (500 µm) was observed for 24h under an inverted microscope (DMI6000B, Leica, Germany) with a live cell imaging system, taking images every 20min. Assay analysis (area covered by cells) was performed with Tscratch.[43]

A-PVA-SPION-labeling of MSCs and A-PVA-SPION dosimetry: Prior use, A-PVA-SPIONs underwent sonication for 1 min and pH-adjustment to neutral range (7.2 - 7.6). Adherent MSCs (80-90% confluence) were washed with PBS and incubated with A-PVA-SPION containing FCS-free culture media for 4h (n=4) with fixed media height (1.3 mm) throughout different culture vessels to prevent variations in the administered dose. Protamine was used at a final concentration of 5 µg/ml (n=2). If MSCs were labeled for 24h (n=2), 10% FCS was added after 4h for sufficient cell nutrition. Finally, A-PVA-labeled MSCs were washed 6x

with PBS before further use. For dosimetry calculations, we used a simplified model based on *In vitro* Sedimentation, Diffusion and Dosimetry model (ISDD) developed by Hinterliter et al., taking additive transport by diffusion and sedimentation into account.[44] The error compared to the ISDD model is reasonably small compared to all the uncertainty arising from the *in vitro* agglomeration and formation of the protein corona, both influencing the diameter and density of the particles. The characteristic properties of the particles used for the calculation of the dose delivered to the cell surface are summarized in Table S2.

Determination of cell-bound iron: After centrifugation at 400xg, the cell pellet was dried overnight at 50°C, re-suspended in 125µl 6N HCL followed by a second overnight incubation step at 50°C. 25µl sample was then mixed with 25µl 6N HCL followed by adding 50µl of 5% $K_4[Fe(CN)_6]$ (Merck, Darmstadt, Germany). After 20min, absorbance was read at 690nm (m200 pro, Tecan, Männedorf, Switzerland) against a standard curve using $FeCl_3$. Each measurement was carried out in quadruplicate. To obtain cell bound iron, iron (pg_{Fe}/cell) was normalized to total cell number (average of 2 x 10^6 cells).

Transmission electron microscopy (TEM) and Transmission X-ray microscopy (TXM):. For TEM, 5x10^5 MSCs were trypsinized and further processed as described previously [45]. After fixation and prior embedding, fixed cells were centrifuged for pellet formation. The mean vesicle size was determined by measuring the diameter of n=4 vesicles from one representative TEM micrograph using ImageJ Software.[46]

For TXM, MSC were cultivated for 24 h on gold grids (type HZB-2, Gilder Grids, Grantham, UK) coated with a perforated carbon film (Quantifoil Micro Tools GmbH, Jena, Germany) prior to A-PVA-SPION-labeling. Samples were then plunge frozen in liquid ethane and transferred into liquid nitrogen. Data acquisition using the HZB TXM at the undulator beamline U41-FSGM, electron storage ring BESSY II, Berlin, was performed as described

previously.[47] For imaging, a zone plate objective with 25 nm outermost zone width was used. The tilt range of the sample was from -60° to +60°. For tomographic reconstruction of the acquired Tilt series eTomo was used and visualized using CTvox (CTvox 2.6, Bruker CT, Kontich, Belgium) for 3D remodeling of the volumetric data.[48] The mean diameter of vesicles and high contrast spheres was determined from seven representative images of the tomograms z-stack using ImageJ Software (vesicles measured: n=9; high contrast spheres measured: n=80).

Visualization by MRI in vitro (phantoms) and in vivo (animals): Female Lewis rats were obtained from Janvier Labs (Cedex, France). The rats weighed between 150 and 175g and were 6-8 weeks old on arrival. They were housed in the animal facility at the University of Geneva under pathogen-free conditions in standard cages and were fed standard diet and water ad libitum. Animal handling was in accordance with guidelines of the Swiss Committee of Animal Experiments. The experimental protocol was approved by the Animal Care Committee at the University of Geneva (authorization no.1049/3580/3). MSC labeling was performed as described. A-PVA-SPION-labeled (100µg_{Fe}/ml) MSCs were trypsinized, counted, and fixed in 4% formaldehyde (Roth, Karlsruhe, Germany). Increasing numbers of fixed cells were spun down and embedded in 200µl 3% (w/v) gelatine on a 48-well plate. The cell phantoms were scanned using the same sequences as optimized for *in vivo* imaging and a 15cm surface for homogeneous signal response. The experiment was carried out on 1.5T scanner. Longer scan times (10 signal averages) were needed to regain the SNR lost going to a larger coil and lower field.

The MR imaging parameters for the phantoms are as followed: A ’T2-weighted’ 2D acquisition with TR/TE/TI 8640/44/160ms, Flip angle 160°, Resolution 0.26 mm, FOV 200*100 mm and slice thickness 1mm. The ’T1-weighted’ gradient echo is a 3D acquisition

with resolution of 0.35mm and slice thickness 0.2mm,TR/TE 22/9.5ms, Flip angle 10° and FOV 160*80mm.

For *in vivo* visualization of labelled cells, the A-PVA-SPION-labeled MSCs and the non-labelled MSCs were injected intra-articularly into the right and left naïve knee joints of Lewis rats (Janvier Labs, Cedex, France) respectively. The following day, MR imaging of rat knee joints in vivo was conducted using a Siemens Magnetom® Trio 3T clinical scanner. A standard 4cm loop coil and respiratory monitoring with a pressure pad were used during the imaging session. The imaging protocol begins with a standard low-resolution localization sequence and the isotropic resolution 3D Ultra-short Echo time (UTE) double echo MR sequence fixed orthogonal and at the magnet centre. This was subsequently used to localize the correct plane for the 2D or thinner slab 3D images as well as for quantitative analysis. The protocol parameters of the sequences used were as follows:

3D T1 gradient echo was used to detect and visualize A-PVA-SPIONs by signal loss. Parameters: TR/TE 14.3/5.9ms, flip angle 12°, fat suppression, isotropic resolution 0.31mm, and FOV 100mm, acquisition time 4 minutes 54 seconds.

Difference Ultra-short Echo time imaging (dUTE) was used for A-PVA-SPION positive contrast detection and quantification. Parameters: 3D isotropic matrix 448 and 80mm FOV, giving 180 µm in all three dimensions, 50000 radial projections, UTE/TE(2) 0.07ms/2.46ms (for in-phase fat/water image), TR 9.6ms (in vivo 100 segments), flip angle 10° , acquisition time 16 minutes 54 seconds.

Statistics: When performing multiple pair-wise comparisons, one-way or two-way analysis of variance (ANOVA) were performed, and p-values were adjusted using Bonferroni's p-value adjustment multiple comparison procedure. Results are presented as mean ± standard deviation (SD). P-values < 0.05 were considered statistically significant.

Supporting Information

Supporting Information is available from the Wiley Online Library or from the author.

Acknowledgements

The research leading to these results has received funding from the European Union Seventh Framework Programme NMP-2008-4.0-1, GRANT AGREEMENT No 228929. We gratefully acknowledge Prof. Petra Knaus and P. Paarmann at the Institute for Chemistry and Biochemistry, Freie Universität Berlin for fruitful discussions and Petra Schrade at the Institute of Vegetative Anatomy, Charité - Universitätsmedizin, Berlin for performing the Transmission electron microscopy analysis. We thank A. Blankenstein, D. Jacobi, L. Schumann, M. Textor and Marie-Gabrielle Beuzelin for excellent technical assistance. MSCs were generously provided by the BCRT Core Unit Cell Harvesting. We thank HZB for the allocation of synchrotron radiation beamtime. We wish to confirm that there are no known conflicts of interest associated with this publication and there has been no significant financial support for this work that could have influenced its outcome.

Received: ((will be filled in by the editorial staff))
Revised: ((will be filled in by the editorial staff))
Published online: ((will be filled in by the editorial staff))

References

[1] Prockop, D. J.; Kota, D. J.; Bazhanov, N.; Reger, R. L., *Journal of cellular and molecular medicine* **2010,** *14* (9), 2190-9. DOI 10.1111/j.1582-4934.2010.01151.x.

[2] Preininger, B.; Duda, G.; Gerigk, H.; Bruckner, J.; Ellinghaus, A.; Sass, F. A.; Perka, C.; Schmidt-Bleek, K.; Dienelt, A., *PloS one* **2013,** *8* (2), e52650. DOI 10.1371/journal.pone.0052650.

[3] Krampera, M.; Pizzolo, G.; Aprili, G.; Franchini, M., *Bone* **2006,** *39* (4), 678-83. DOI 10.1016/j.bone.2006.04.020.

[4] Chanda, D.; Kumar, S.; Ponnazhagan, S., *Journal of cellular biochemistry* **2010,** *111* (2), 249-57. DOI 10.1002/jcb.22701.

[5] Chen, F. H.; Tuan, R. S., *Arthritis research & therapy* **2008,** *10* (5), 223. DOI 10.1186/ar2514.

[6] Stamm, C.; Klose, K.; Choi, Y. H., *Advances in biochemical engineering/biotechnology* **2010,** *123*, 293-317. DOI 10.1007/10_2010_77.

[7] Naegele, J. R.; Maisano, X.; Yang, J.; Royston, S.; Ribeiro, E., *Neuropharmacology* **2010,** *58* (6), 855-64. DOI 10.1016/j.neuropharm.2010.01.019.

[8] Chiu, A. Y.; Rao, M. S., *Neurotherapeutics : the journal of the American Society for Experimental NeuroTherapeutics* **2011,** *8* (4), 744-52. DOI 10.1007/s13311-011-0066-9.

[9] Salem, H. K.; Thiemermann, C., *Stem Cells* **2010,** *28* (3), 585-96. DOI 10.1002/stem.269.

[10] Bhirde, A.; Xie, J.; Swierczewska, M.; Chen, X., *Nanoscale* **2011,** *3* (1), 142-53. DOI 10.1039/c0nr00493f.

[11] Tang, F.; Barbacioru, C.; Bao, S.; Lee, C.; Nordman, E.; Wang, X.; Lao, K.; Surani, M. A., *Cell stem cell* **2010,** *6* (5), 468-78. DOI 10.1016/j.stem.2010.03.015.

[12] Schafer, R.; Kehlbach, R.; Muller, M.; Bantleon, R.; Kluba, T.; Ayturan, M.; Siegel, G.; Wolburg, H.; Northoff, H.; Dietz, K.; Claussen, C. D.; Wiskirchen, J., *Cytotherapy* **2009,** *11* (1), 68-78. DOI 10.1080/14653240802666043.

[13] Corot, C.; Robert, P.; Idee, J. M.; Port, M., *Advanced drug delivery reviews* **2006,** *58* (14), 1471-504. DOI 10.1016/j.addr.2006.09.013.

[14] Gossuin, Y.; Gillis, P.; Hocq, A.; Vuong, Q. L.; Roch, A., *Wiley interdisciplinary reviews. Nanomedicine and nanobiotechnology* **2009,** *1* (3), 299-310. DOI 10.1002/wnan.36.

[15] Gupta, A. K.; Gupta, M., *Biomaterials* **2005,** *26* (18), 3995-4021. DOI 10.1016/j.biomaterials.2004.10.012.

[16] Schafer, R.; Ayturan, M.; Bantleon, R.; Kehlbach, R.; Siegel, G.; Pintaske, J.; Conrad, S.; Wolburg, H.; Northoff, H.; Wiskirchen, J.; Weissert, R., *Cell transplantation* **2008,** *17* (8), 923-41.

[17] Arbab, A. S.; Yocum, G. T.; Kalish, H.; Jordan, E. K.; Anderson, S. A.; Khakoo, A. Y.; Read, E. J.; Frank, J. A., *Blood* **2004,** *104* (4), 1217-23. DOI 10.1182/blood-2004-02-0655.

[18] Kostura, L.; Kraitchman, D. L.; Mackay, A. M.; Pittenger, M. F.; Bulte, J. W., *NMR in biomedicine* **2004,** *17* (7), 513-7. DOI 10.1002/nbm.925.

[19] Henning, T. D.; Sutton, E. J.; Kim, A.; Golovko, D.; Horvai, A.; Ackerman, L.; Sennino, B.; McDonald, D.; Lotz, J.; Daldrup-Link, H. E., *Contrast media & molecular imaging* **2009,** *4* (4), 165-73. DOI 10.1002/cmmi.276.

[20] van Buul, G. M.; Farrell, E.; Kops, N.; van Tiel, S. T.; Bos, P. K.; Weinans, H.; Krestin, G. P.; van Osch, G. J.; Bernsen, M. R., *Contrast media & molecular imaging* **2009,** *4* (5), 230-6. DOI 10.1002/cmmi.289.

[21] Ittrich, H.; Lange, C.; Togel, F.; Zander, A. R.; Dahnke, H.; Westenfelder, C.; Adam, G.; Nolte-Ernsting, C., *Journal of magnetic resonance imaging : JMRI* **2007,** *25* (6), 1179-91. DOI 10.1002/jmri.20925.

[22] Vallee, J. P.; Hauwel, M.; Lepetit-Coiffe, M.; Bei, W.; Montet-Abou, K.; Meda, P.; Gardier, S.; Zammaretti, P.; Kraehenbuehl, T. P.; Herrmann, F.; Hubbell, J. A.; Jaconi, M. E., *Stem cells translational medicine* **2012,** *1* (3), 248-60. DOI 10.5966/sctm.2011-0028.

[23] Frank, J. A.; Miller, B. R.; Arbab, A. S.; Zywicke, H. A.; Jordan, E. K.; Lewis, B. K.; Bryant, L. H., Jr.; Bulte, J. W., *Radiology* **2003,** *228* (2), 480-7. DOI 10.1148/radiol.2281020638.

[24] Arbab, A. S.; Yocum, G. T.; Rad, A. M.; Khakoo, A. Y.; Fellowes, V.; Read, E. J.; Frank, J. A., *NMR in biomedicine* **2005,** *18* (8), 553-9. DOI 10.1002/nbm.991.

[25] Bulte, J. W.; Kraitchman, D. L.; Mackay, A. M.; Pittenger, M. F., *Blood* **2004,** *104* (10), 3410-2; author reply 3412-3. DOI 10.1182/blood-2004-06-2117.

[26] Balakumaran, A.; Pawelczyk, E.; Ren, J.; Sworder, B.; Chaudhry, A.; Sabatino, M.; Stroncek, D.; Frank, J. A.; Robey, P. G., *PloS one* **2010,** *5* (7), e11462. DOI 10.1371/journal.pone.0011462.
[27] Singh, N.; Jenkins, G. J.; Asadi, R.; Doak, S. H., *Nano reviews* **2010,** *1*. DOI 10.3402/nano.v1i0.5358.
[28] Delcroix, G. J.; Jacquart, M.; Lemaire, L.; Sindji, L.; Franconi, F.; Le Jeune, J. J.; Montero-Menei, C. N., *Brain research* **2009,** *1255*, 18-31. DOI 10.1016/j.brainres.2008.12.013.
[29] Reddy, A. M.; Kwak, B. K.; Shim, H. J.; Ahn, C.; Cho, S. H.; Kim, B. J.; Jeong, S. Y.; Hwang, S. J.; Yuk, S. H., *Contrast media & molecular imaging* **2009,** *4* (3), 118-26. DOI 10.1002/cmmi.271.
[30] Chen, C. L.; Zhang, H.; Ye, Q.; Hsieh, W. Y.; Hitchens, T. K.; Shen, H. H.; Liu, L.; Wu, Y. J.; Foley, L. M.; Wang, S. J.; Ho, C., *Molecular imaging and biology : MIB : the official publication of the Academy of Molecular Imaging* **2011,** *13* (5), 825-39. DOI 10.1007/s11307-010-0430-x.
[31] Landazuri, N.; Tong, S.; Suo, J.; Joseph, G.; Weiss, D.; Sutcliffe, D. J.; Giddens, D. P.; Bao, G.; Taylor, W. R., *Small* **2013,** *9* (23), 4017-26. DOI 10.1002/smll.201300570.
[32] Wang, L.; Neoh, K. G.; Kang, E. T.; Shuter, B.; Wang, S. C., *Biomaterials* **2010,** *31* (13), 3502-11. DOI 10.1016/j.biomaterials.2010.01.081.
[33] Xu, C.; Miranda-Nieves, D.; Ankrum, J. A.; Matthiesen, M. E.; Phillips, J. A.; Roes, I.; Wojtkiewicz, G. R.; Juneja, V.; Kultima, J. R.; Zhao, W.; Vemula, P. K.; Lin, C. P.; Nahrendorf, M.; Karp, J. M., *Nano letters* **2012,** *12* (8), 4131-9. DOI 10.1021/nl301658q.
[34] Khanbeigi, R. A.; Kumar, A.; Sadouki, F.; Lorenz, C.; Forbes, B.; Dailey, L. A.; Collins, H., *Journal of Controlled Release* **2012,** *162* (2), 259-266. DOI DOI 10.1016/j.jconrel.2012.07.019.
[35] Dominici, M.; Le Blanc, K.; Mueller, I.; Slaper-Cortenbach, I.; Marini, F.; Krause, D.; Deans, R.; Keating, A.; Prockop, D.; Horwitz, E., *Cytotherapy* **2006,** *8* (4), 315-7. DOI 10.1080/14653240600855905.
[36] Chastellain, M.; Petri, A.; Hofmann, H., *Journal of colloid and interface science* **2004,** *278* (2), 353-60. DOI 10.1016/j.jcis.2004.06.025.
[37] Massart, R.; Dubois, E.; Cabuil, V.; Hasmonay, E., *J Magn Magn Mater* **1995,** *149* (1-2), 1-5. DOI Doi 10.1016/0304-8853(95)00316-9.
[38] Petri-Fink, A.; Chastellain, M.; Juillerat-Jeanneret, L.; Ferrari, A.; Hofmann, H., *Biomaterials* **2005,** *26* (15), 2685-94. DOI 10.1016/j.biomaterials.2004.07.023.
[39] Schulze, K.; Koch, A.; Schopf, B.; Petri, A.; Steitz, B.; Chastellain, M.; Hofmann, M.; Hofmann, H.; von Rechenberg, B., *J Magn Magn Mater* **2005,** *293* (1), 419-432. DOI DOI 10.1016/j.jmmm.2005.02.075.
[40] Ode, A.; Duda, G. N.; Glaeser, J. D.; Matziolis, G.; Frauenschuh, S.; Perka, C.; Wilson, C. J.; Kasper, G., *Journal of biomedical materials research. Part A* **2010,** *95* (4), 1114-24. DOI 10.1002/jbm.a.32909.
[41] Geissler, S.; Textor, M.; Kuhnisch, J.; Konnig, D.; Klein, O.; Ode, A.; Pfitzner, T.; Adjaye, J.; Kasper, G.; Duda, G. N., *PloS one* **2012,** *7* (12), e52700. DOI 10.1371/journal.pone.0052700.
[42] Davis, L. A.; Dienelt, A.; zur Nieden, N. I., *Methods Mol Biol* **2011,** *690*, 255-72. DOI 10.1007/978-1-60761-962-8_17.
[43] Geback, T.; Schulz, M. M.; Koumoutsakos, P.; Detmar, M., *BioTechniques* **2009,** *46* (4), 265-74. DOI 10.2144/000113083.
[44] Hinderliter, P. M.; Minard, K. R.; Orr, G.; Chrisler, W. B.; Thrall, B. D.; Pounds, J. G.; Teeguarden, J. G., *Particle and fibre toxicology* **2010,** *7* (1), 36. DOI 10.1186/1743-8977-7-36.
[45] Ode, A.; Kopf, J.; Kurtz, A.; Schmidt-Bleek, K.; Schrade, P.; Kolar, P.; Buttgereit, F.; Lehmann, K.; Hutmacher, D. W.; Duda, G. N.; Kasper, G., *European cells & materials* **2011,** *22*, 26-42.
[46] Schneider, C. A.; Rasband, W. S.; Eliceiri, K. W., *Nature methods* **2012,** *9* (7), 671-5.
[47] Schneider, G.; Guttmann, P.; Heim, S.; Rehbein, S.; Mueller, F.; Nagashima, K.; Heymann, J. B.; Muller, W. G.; McNally, J. G., *Nature methods* **2010,** *7* (12), 985-7. DOI 10.1038/nmeth.1533.
[48] Kremer, J. R.; Mastronarde, D. N.; McIntosh, J. R., *Journal of structural biology* **1996,** *116* (1), 71-6. DOI 10.1006/jsbi.1996.0013.
[49] Lesniak, A.; Fenaroli, F.; Monopoli, M. P.; Aberg, C.; Dawson, K. A.; Salvati, A., *ACS nano* **2012,** *6* (7), 5845-57. DOI 10.1021/nn300223w.

[50] Schrurs, F.; Lison, D., *Nature nanotechnology* **2012,** *7* (9), 546-8. DOI 10.1038/nnano.2012.148.
[51] Monopoli, M. P.; Walczyk, D.; Campbell, A.; Elia, G.; Lynch, I.; Bombelli, F. B.; Dawson, K. A., *Journal of the American Chemical Society* **2011,** *133* (8), 2525-34. DOI 10.1021/ja107583h.
[52] Petri-Fink, A.; Steitz, B.; Finka, A.; Salaklang, J.; Hofmann, H., *European journal of pharmaceutics and biopharmaceutics : official journal of Arbeitsgemeinschaft fur Pharmazeutische Verfahrenstechnik e.V* **2008,** *68* (1), 129-37. DOI 10.1016/j.ejpb.2007.02.024.
[53] Teeguarden, J. G.; Hinderliter, P. M.; Orr, G.; Thrall, B. D.; Pounds, J. G., *Toxicological sciences : an official journal of the Society of Toxicology* **2007,** *95* (2), 300-12. DOI 10.1093/toxsci/kfl165.
[54] Baker, M. I.; Walsh, S. P.; Schwartz, Z.; Boyan, B. D., *Journal of biomedical materials research. Part B, Applied biomaterials* **2012,** *100* (5), 1451-7. DOI 10.1002/jbm.b.32694.
[55] Petri-Fink, A.; Hofmann, H., *IEEE transactions on nanobioscience* **2007,** *6* (4), 289-97.
[56] Chung, T. H.; Wu, S. H.; Yao, M.; Lu, C. W.; Lin, Y. S.; Hung, Y.; Mou, C. Y.; Chen, Y. C.; Huang, D. M., *Biomaterials* **2007,** *28* (19), 2959-66. DOI 10.1016/j.biomaterials.2007.03.006.
[57] Cengelli, F.; Maysinger, D.; Tschudi-Monnet, F.; Montet, X.; Corot, C.; Petri-Fink, A.; Hofmann, H.; Juillerat-Jeanneret, L., *The Journal of pharmacology and experimental therapeutics* **2006,** *318* (1), 108-16. DOI 10.1124/jpet.106.101915.
[58] Cartiera, M. S.; Johnson, K. M.; Rajendran, V.; Caplan, M. J.; Saltzman, W. M., *Biomaterials* **2009,** *30* (14), 2790-8. DOI 10.1016/j.biomaterials.2009.01.057.
[59] Andreas, K.; Georgieva, R.; Ladwig, M.; Mueller, S.; Notter, M.; Sittinger, M.; Ringe, J., *Biomaterials* **2012,** *33* (18), 4515-25. DOI 10.1016/j.biomaterials.2012.02.064.
[60] Oyama, M.; Tatlock, A.; Fukuta, S.; Kavalkovich, K.; Nishimura, K.; Johnstone, B.; Robbins, P. D.; Evans, C. H.; Niyibizi, C., *Gene therapy* **1999,** *6* (3), 321-9. DOI 10.1038/sj.gt.3300839.
[61] Shirley, D.; Marsh, D.; Jordan, G.; McQuaid, S.; Li, G., *Journal of orthopaedic research : official publication of the Orthopaedic Research Society* **2005,** *23* (5), 1013-21. DOI 10.1016/j.orthres.2005.01.013.
[62] Granero-Molto, F.; Weis, J. A.; Miga, M. I.; Landis, B.; Myers, T. J.; O'Rear, L.; Longobardi, L.; Jansen, E. D.; Mortlock, D. P.; Spagnoli, A., *Stem Cells* **2009,** *27* (8), 1887-98. DOI 10.1002/stem.103.

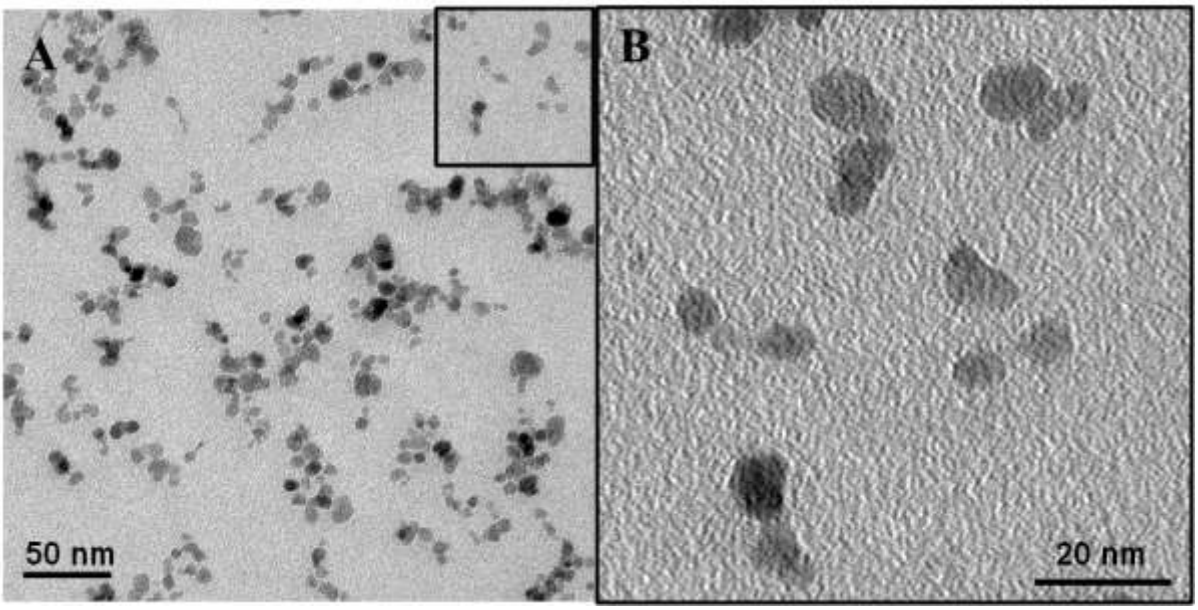

Figure 1. TEM pictures of A-PVA-SPIONs. (A+B) TEM micrographs show iron oxide cores from A-PVA-SPIONs and were used to determine the mean average size of the ɣ Fe_2O_3 crystals

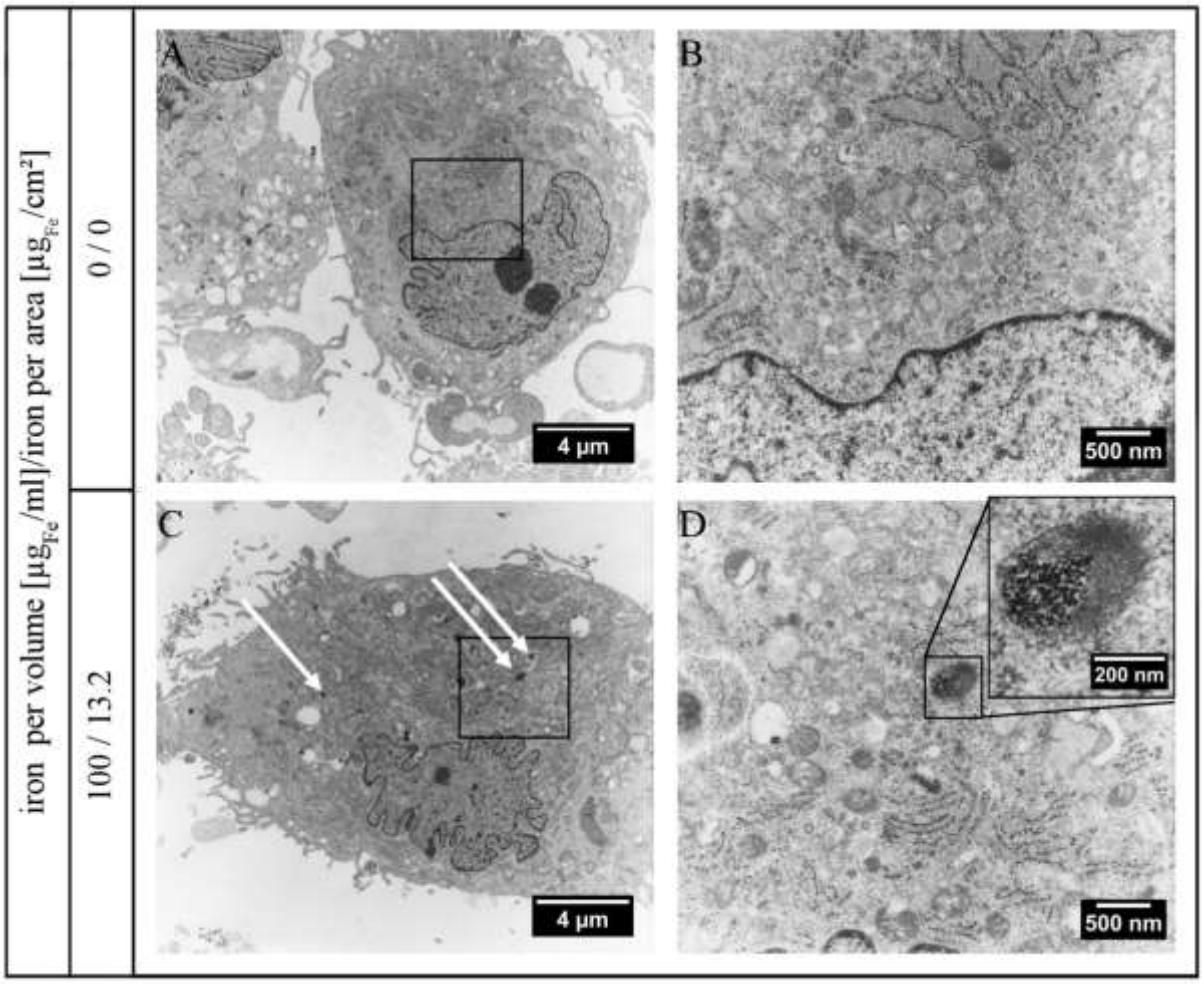

Figure 2. A-PVA-SPIONs are internalized by MSCs that store them in intracellular vesicles. Shown are two representative pictures of (A, B) non-labeled and (C, D) A-PVA-labeled MSCs at different magnification detection by TEM. A-PVA-SPIONs are visible as intra-vesicular colloids (white arrows) in labeled MSCs that are absent in unlabeled control cells.

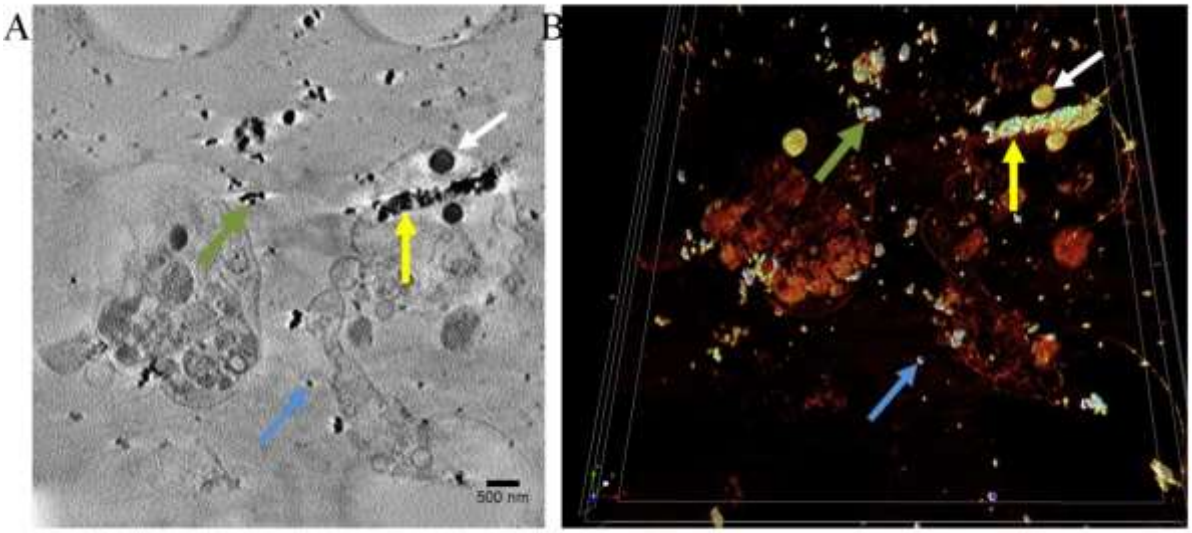

Figure 3. Internalized A-PVA-SPIONs are differently distributed in cytoplasm. The acquired tilt series of A-PVA-SPION-labeled MSCs by TXM allowed tomographic reconstruction. Shown are (A) one slice from z-stack and (B) subsequent 3D modeling. A-PVA-SPIONs are visible not only as intravesicular colloids (white arrows), but also as smaller high contrast spheres (blue arrows), clusters of irregular shape (green arrows), and as a micron-sized cluster (yellow arrow) in the cytoplasm.

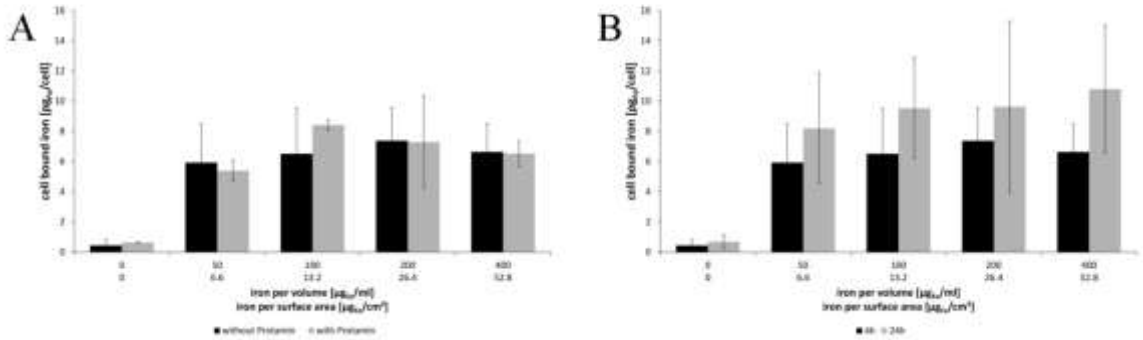

Figure 4. Efficient labeling of MSCs with A-PVA-SPIONs can be achieved at low administered doses and does not require Protamine. MSCs were incubated with A-PVA-SPIONs (A) for 4h with and without Protamine under serum-free conditions and (B) for 24h in the absence of Protamine.

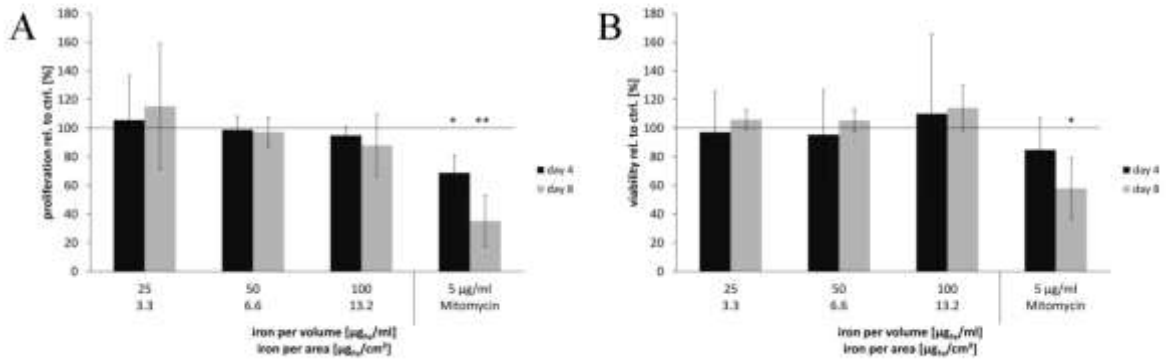

Figure 5. Proliferation and viability of MSCs are not affected by A-PVA-SPION-labeling. (A) Proliferation and (B) viability of A-PVA-SPION-labeled MSCs was assessed after four and eight days.

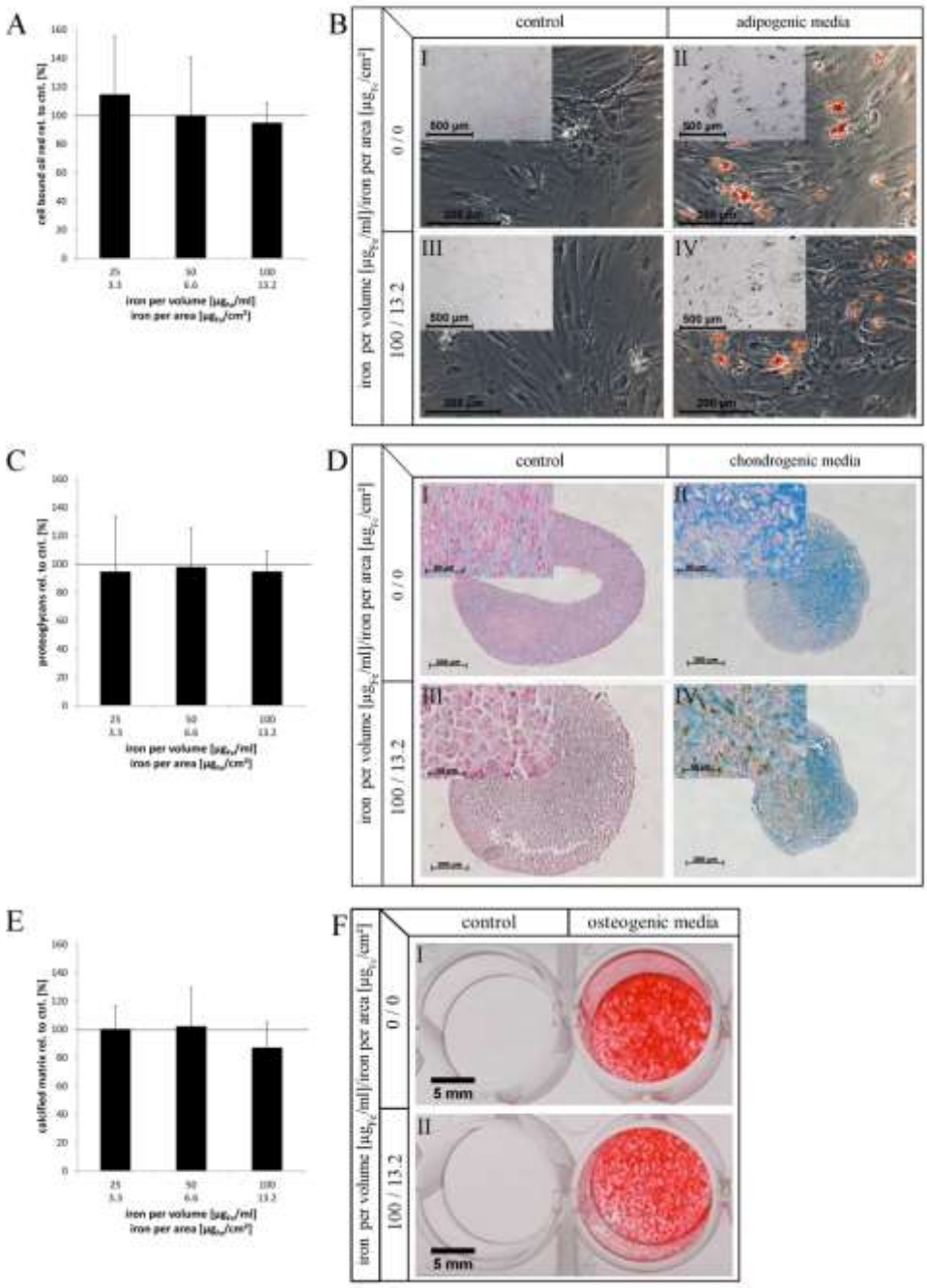

680

681 **Figure 6. Differentiation capacity of MSCs is not influenced by A-PVA-SPIONs.** A-PVA-
682 SPION–labeled MSCs were (A+C+E) quantitatively and (B+D+F) qualitatively investigated
683 towards (A+B) adipogenic differentiation by Oil red staining(C+D) chondrogenic
684 differentiation by proteoglycan assay and Alcian blue staining, and (E+F) osteogenic
685 differentiation by Alizarin red staining.

686
687

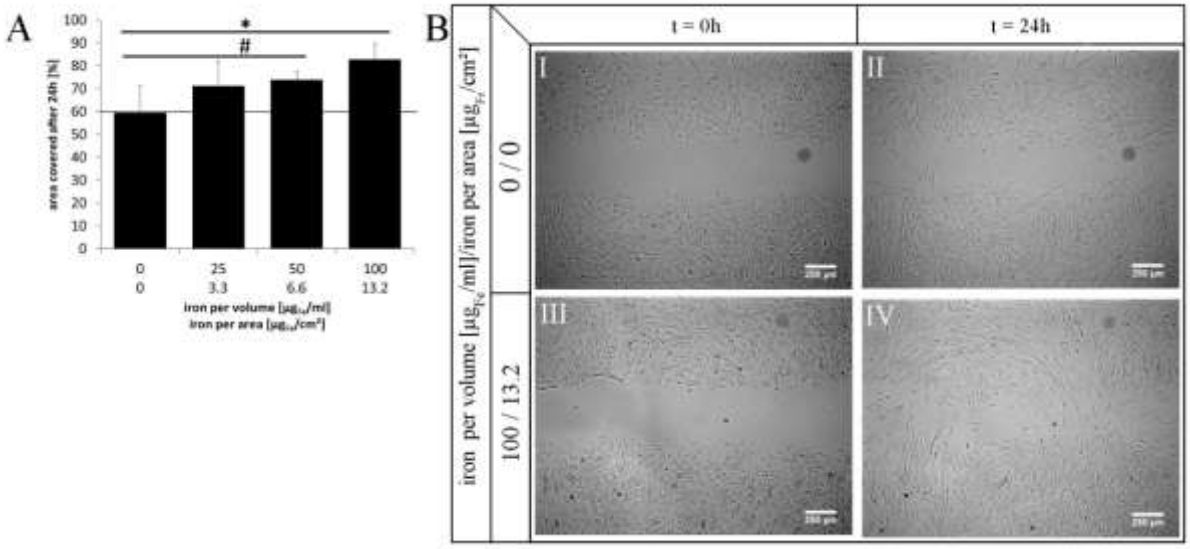

688

689 **Figure 7. Migration of MSCs is stimulated by A-PVA-SPION-labeling.** (A) Migration of
690 A-PVA-SPION-labeled MSCs was investigated in a wound healing assay for 24h (ANOVA,
691 Post Hoc Bonferoni; *, p = 0.001; #, p = 0.069). (B) Representative images of the wound
692 healing gap from one donor are shown.

693
694

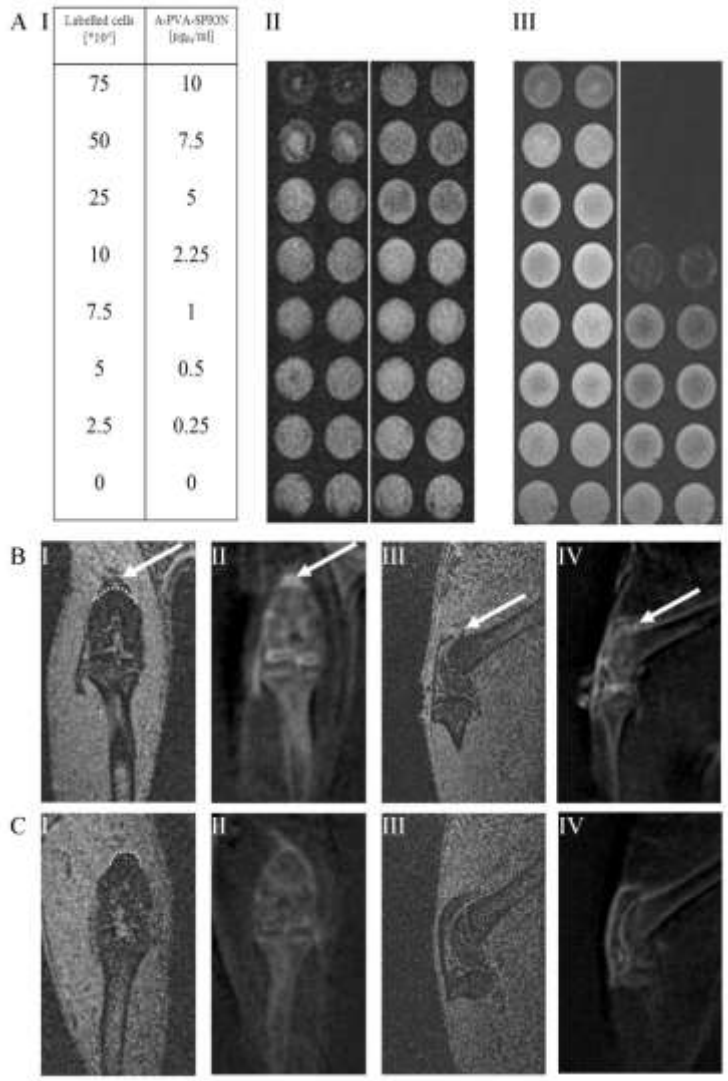

Figure 8. Visualization of A-PVA-labeled MSCs in MRI *in vitro* and *in vivo*. (A) A diagrammatic representation showing the layout and the different concentrations of A-PVA-SPION labeled MSCs and SPION alone used in the 24-well plate gel phantom study (I). T1 weighted gradient echo MR images of the gel phantom (II) and T2 weighted (STIR) MR images of the same gel phantom (III). (B) Coronal (I, II) and sagittal (III, IV) views of rat knee joint injected with A-PVA-SPION labeled MSCs and scanned *in vivo*. (C) Coronal (I, II) and sagittal (III, IV) views of rat knee joint injected with non labeled MSCs and scanned *in vivo*. Phantom was scanned using 1.5T MRI, rat knees were scanned *in vivo* using a 3T MRI. White arrow: A-PVA-SPION labeled MSCs. Dotted white line: contour of the femoral diaphysis.

Table 1. Physiochemical properties of A-PVA-SPIONs in different solvents

Particles	Medium	Concentration (mg_{Fe}/mL)	γ Fe_2O_3 chrystal (nm)	Hydrodynamic diameter (nm)	Zeta potential (mV)	PVA/Fe ratio (mg_{PVA}/mg_{Fe})
SPION	HNO_3 10mM	10	7.2 ± 2.5	14 ± 2	+26 ± 2	0
PVA-SPION	HNO_3 10mM	5	7.2 ± 2.5	25 ± 3	+20 ± 2	9
PVA-SPION	DMEM	5	7.2 ± 2.5	42 ± 2	+21 ± 5	9
PVA-SPION	DMEM+FCS	5	7.2 ± 2.5	45 ± 2	-25 ± 5	9

Table 2. Dosimetry

administered dose						
iron per volume [μg_{Fe}/ml]		0	50	100	200	400
iron per area [$\mu g_{Fe}/cm^2$]		0	6.6	13.2	26.4	52.8
delivered dose						
iron per area [$\mu g_{Fe}/cm^2$]	4h	0	0.9	1.6	3.1	6.2
	24h	0	2.3	4.1	7.9	15.3
iron per cell [pg_{Fe}/cell]	4h	0	3	6	12	24
	24h	0	7.5	15	30	60
cellular dose						
iron per cell [pg_{Fe}/cell]	4h	0.4 ± 0.3	5.9 ± 2.5	6.5 ± 3.0	7.4 ± 2.2	6.6 ± 1.9
	24h	0.7 ± 0.5	8.2 ± 3.6	9.5 ± 3.3	9.6 ± 5.7	10.8 ± 4.2

Table of content

Amino-polyvinyl alcohol coated superparamagnetic iron oxide nanoparticles (A-PVA-SPIONs) were used to label mesenchymal stromal cells (MSCs) for visualization in magnetic resonance imaging. The A-PVA-SPIONs were non-toxic to MSCs and did not change their differentiation potential. However, an increase in MSCs migration was observed. In conclusion, labeling MSCs using A-PVA-SPIONs is feasible.

Keyword: mesenchymal stromal cells, superparamagnetic iron oxide nanoparticles, polyvinylalcohol, magnetic resonance imaging, cell based therapies

Frank Schulze, Anke Dienelt, Sven Geissler, Paul Zaslansky, Janosch Schoon, Katja Henzler, Peter Guttmann, Azza Gramoun, Lindsey A. Crowe, Lionel Maurizi, Jean-Paul Vallée, Heinrich Hofmann, Georg N. Duda*, Andrea Ode

Title

Amino-polyvinyl alcohol coated superparamagnetic iron oxide nanoparticles are suitable for monitoring of human mesenchymal stromal cells *in vivo*

ToC figure ((Please choose one size: 55 mm broad × 50 mm high or 110 mm broad × 20 mm high. Please do not use any other dimensions))